SCHRIFTENREIHE DES FACHBEREICHS MATHEMATIK

Robust FETI-DP Methods for Heterogeneous Three Dimensional Elasticity Problems

by

Axel Klawonn and Oliver Rheinbach

SM-E-607 2005

Universität Duisburg-Essen

Eingegangen am 11.07.2005

ROBUST FETI-DP METHODS FOR HETEROGENEOUS THREE DIMENSIONAL ELASTICITY PROBLEMS

AXEL KLAWONN* AND OLIVER RHEINBACH*

July 2005

Abstract. Iterative substructuring methods with Lagrange multipliers are considered for heterogeneous linear elasticity problems with large discontinuities in the material stiffnesses. In particular, results for algorithms belonging to the family of dual-primal FETI methods are presented. The core issue of these algorithms is the construction of an appropriate global problem, in order to obtain a robust method which converges independently of the material discontinuities. In this article, several necessary and sufficient conditions arising from the theory are numerically tested and confirmed. Furthermore, results of numerical experiments are presented for situation which are not covered by the theory, such as curved edges and material discontinuities not aligned with the interface, and an attempt is made to develop rules for these cases.

Key words. domain decomposition, Lagrange multipliers, FETI, preconditioners, elliptic systems, elasticity, finite elements, parallel computing.

AMS subject classifications. 65F10, 65N30, 65N55

1. Introduction. Domain decomposition methods provide a good approach to obtaining robust and parallel scalable solvers for the large systems of equations arising from the discretization of elasticity problems. Here, we will consider algorithms which belong to the family of dual-primal FETI (finite element tearing and interconnecting) methods, see, e.g., [7], [8], [11], [9], or [18]. Dual-primal FETI (FETI-DP) methods are iterative substructuring algorithms with Lagrange multipliers where some continuity constraints on primal displacement variables are required to hold throughout the iterations, as in standard iterative substructuring methods, while most of the constraints are enforced by the use of dual Lagrange multipliers. The primal constraints should be chosen so that the local problems become invertible. They also provide a coarse problem and should be selected so that the iterative method converges rapidly. Recently, the family of algorithms for linear elasticity problems in three dimensions was extended and a theory was provided in [11]. It was shown that the condition number of the dual-primal FETI methods can be bounded polylogarithmically as a function of the dimension of the individual subregion problems and that the bounds can otherwise be made independent of the number of subdomains, the mesh size, and jumps in the coefficients. Special emphasis was given in [11] on developing robust condition number estimates with bounds which are independent of arbitrarily large jumps of the material coefficients. For benign coefficients, without large jumps, it is sufficient to select an appropriate set of edge averages as primal constraints to obtain good bounds, whereas for arbitrary coefficient distributions, additional primal first order moments and constraints at some of the vertices are also required. Extensive experimental work on dual-primal FETI methods for homogeneous linear elasticity problems is reported on in Klawonn and Rheinbach [9]. The results given in [9] confirm the theoretical analysis in [11] and show the good scalability properties of our algorithms for model problems as well as for industrial applications.

In the present article, we will instead focus on heterogeneous elasticity problems

*Fachbereich Mathematik, Universität Duisburg-Essen, Universitätsstr. 3, D-45117 Essen, Germany. E-mail: axel.klawonn@uni-essen.de,oliver.rheinbach@uni-essen.de, WWW: http://www.uni-essen.de/numa

with large discontinuities in the material stiffnesses. In [11], it was shown that selecting certain edge averages and first order moments and, in some very hard cases, certain vertices as primal constraints, yields a robust condition number estimate. The central assumption is that on every face, we can control the rigid body modes and additionally, certain theoretical estimates are satisfied; cf. [11, Section 5]. We now provide numerical results which confirm the theoretical findings in [11] and show that in some cases, first order moments are indeed necessary to obtain a good convergence rate. In the theory of [11], it is assumed that the edges of the subdomains are straight and that large material discontinuities are aligned with the subdomain boundaries. We relax these assumptions and provide numerical results for decompositions with curved edges and with material discontinuities which are not aligned with the interface. We note that a short conference paper [10] prepared previously, provides some preliminary results on FETI-DP algorithms applied to heterogeneous problems.

We expect that our numerical results also provide insight into the performance of the more recently developed Neumann-Neumann methods with constraints, known as the BDDC algorithms, cf. [6, 15, 16, 14], since Mandel, Dohrmann, and Tezaur [16] have shown that, for any given set of constraints, the BDDC and FETI-DP methods have almost all their eigenvalues in common; see also Li and Widlund [14] for an alternative proof.

The remainder of this article is organized as follows. In Section 2, we introduce the problem of linear elasticity, its discretization by finite elements, and the basic assumptions on our domain decomposition. In the following Section 3, we introduce our FETI-DP algorithm and provide a theoretical condition number estimate from [11]. In Section 4, we present results of computational experiments, which help to identify necessary and sufficient constraint conditions in order to obtain robust algorithms. In Section 5, we consider a model problem with curved edges, to identify the effect on condition and iteration numbers numerically, since it cannot be captured by the standard theoretical arguments. In Section 6, we show the effects of material inhomogeneities which are not aligned with the interface and consider different model situations together with possible remedies. Finally, we present our conclusions in Section 7.

2. Linear elasticity and finite elements. The equations of linear elasticity model the displacement of a linear elastic material under the action of external and internal forces. The elastic body occupies a domain $\Omega \subset \mathbb{R}^3$. We denote its boundary by $\partial\Omega$ and assume that one part of it, $\partial\Omega_D$, is clamped, i.e., with homogeneous Dirichlet boundary conditions, and that the rest, $\partial\Omega_N := \partial\Omega \setminus \partial\Omega_D$, is subject to a surface force $\mathbf{g}$, i.e., a natural boundary condition. We can also introduce a body force $\mathbf{f}$, e.g., gravity. With $\mathbf{H^1}(\Omega) := (H^1(\Omega))^3$, the appropriate space for a variational formulation is the Sobolev space $\mathbf{H^1_0}(\Omega, \partial\Omega_D) := \{\mathbf{v} \in \mathbf{H^1}(\Omega) : \mathbf{v} = \mathbf{0} \text{ on } \partial\Omega_D\}$. The linear elasticity problem consists in finding the displacement $\mathbf{u} \in \mathbf{H^1_0}(\Omega, \partial\Omega_D)$ of the elastic body Ω, such that

$$\int_\Omega G(\mathbf{x})\varepsilon(\mathbf{u}) : \varepsilon(\mathbf{v}) d\mathbf{x} + \int_\Omega G(\mathbf{x})\,\beta(\mathbf{x})\,\mathrm{div}\mathbf{u}\,\mathrm{div}\mathbf{v}\,d\mathbf{x} = \langle \mathbf{F}, \mathbf{v}\rangle \;\; \forall \mathbf{v} \in \mathbf{H^1_0}(\Omega, \partial\Omega_D). \quad (2.1)$$

Here G and β are material parameters which depend on the Young modulus $E > 0$ and the Poisson ratio $\nu \in (0, 1/2]$; we have $G = E/(1+\nu)$ and $\beta = \nu/(1-2\nu)$. In this article, we only consider the case of compressible elasticity, which means that the Poisson ratio ν is bounded away from $1/2$. Furthermore, $\varepsilon_{ij}(\mathbf{u}) := \frac{1}{2}(\frac{\partial u_i}{\partial x_j} + \frac{\partial u_j}{\partial x_i})$ is

the linearized strain tensor, and

$$\varepsilon(\mathbf{u}) : \varepsilon(\mathbf{v}) = \sum_{i,j=1}^{3} \varepsilon_{ij}(\mathbf{u})\varepsilon_{ij}(\mathbf{v}), \quad \langle \mathbf{F}, \mathbf{v} \rangle := \int_{\Omega} \mathbf{f}^T \mathbf{v} \, d\mathbf{x} \; + \; \int_{\partial\Omega_N} \mathbf{g}^T \mathbf{v} \, d\sigma.$$

For convenience, we also introduce the notation

$$(\varepsilon(\mathbf{u}), \varepsilon(\mathbf{v}))_{L_2(\Omega)} := \int_{\Omega} \varepsilon(\mathbf{u}) : \varepsilon(\mathbf{v}) d\mathbf{x}.$$

The bilinear form associated with linear elasticity is then

$$a(\mathbf{u}, \mathbf{v}) = (G\,\varepsilon(\mathbf{u}), \varepsilon(\mathbf{v}))_{L_2(\Omega)} \; + \; (G\,\beta\,\mathrm{div}\mathbf{u}, \mathrm{div}\mathbf{v})_{L_2(\Omega)}.$$

The wellposedness of the linear system (2.1) follows immediately from the continuity and ellipticity of the bilinear form $a(\cdot, \cdot)$, where the first follows from elementary inequalities and the latter from Korn's first inequality; see, e.g., [4]. The null space $\mathbf{ker}\,(\varepsilon)$ of ε is the space of the six rigid body motions, which is spanned by the three translations $\mathbf{r}_i := \mathbf{e}_i, i = 1, 2, 3$, where the $\mathbf{e}_i$ are the three standard unit vectors, and the three rotations

$$\mathbf{r}_4 := \begin{bmatrix} x_2 - \hat{x}_2 \\ -x_1 + \hat{x}_1 \\ 0 \end{bmatrix}, \mathbf{r}_5 := \begin{bmatrix} -x_3 + \hat{x}_3 \\ 0 \\ x_1 - \hat{x}_1 \end{bmatrix}, \mathbf{r}_6 := \begin{bmatrix} 0 \\ x_3 - \hat{x}_3 \\ -x_2 + \hat{x}_2 \end{bmatrix}. \tag{2.2}$$

Here, we have $\hat{\mathbf{x}} \in \Omega$ to shift the origin to a point in Ω.

We will only consider compressible elastic materials. It is therefore sufficient to discretize our elliptic problem of linear elasticity (2.1) by low order, conforming finite elements, e.g., linear or trilinear elements.

Let us assume that a triangulation τ^h of Ω is given which is shape regular and has a typical diameter of h. We denote by $\mathbf{W}^h := \mathbf{W}^h(\Omega)$ the corresponding conforming finite element space of finite element functions. The associated discrete problem is then

$$a(\mathbf{u}_h, \mathbf{v}_h) = \langle \mathbf{F}, \mathbf{v}_h \rangle \quad \forall \mathbf{v}_h \in \mathbf{W}^h. \tag{2.3}$$

When there is no risk of confusion, we will drop the subscript h.

Let the domain $\Omega \subset \mathbb{R}^3$ be decomposed into nonoverlapping subdomains $\Omega_i, i = 1, \ldots, N$, each of which is the union of finite elements with matching finite element nodes on the boundaries of neighboring subdomains across the interface Γ. The interface Γ is the union of three different types of open sets, namely, subdomain faces, edges, and vertices. We denote individual faces, edges, and vertices by $\mathcal{F}, \mathcal{E}$, and $\mathcal{V}$, respectively. For the case of regular substructures such as cubes or tetrahedrons, we can use the standard geometric definition of faces, edges, and vertices. To define faces, edges, and vertices more generally, we introduce certain equivalence classes; cf. [11] or [9]. Let us denote the sets of nodes on $\partial\Omega$, $\partial\Omega_i$, and Γ by $\partial\Omega_h$, $\partial\Omega_{i,h}$, and Γ_h, respectively. For any interface nodal point $x \in \Gamma_h$, we define

$$\mathcal{N}_x := \{j \in \{1, \ldots, N\} : x \in \partial\Omega_j\},$$

i.e., $\mathcal{N}_x$ is the set of indices of all subdomains with x in the closure of the subdomain. For a node x we define the multiplicity as $|N_x|$.

Associated with the nodes of the finite element mesh, we have a graph, the nodal graph, which represents the node-to-node adjacency. For a given node $x \in \Gamma_h$, we denote by $\mathcal{C}_{con}(x)$ the connected component of the nodal subgraph, defined by $\mathcal{N}_x$, to which x belongs. For two interface points $x, y \in \Gamma_h$, we introduce an equivalence relation by

$$x \sim y :\Longleftrightarrow \mathcal{N}_x = \mathcal{N}_y \text{ and } y \in \mathcal{C}_{con}(x).$$

We can now describe faces, edges, and vertices using their equivalence classes. Here, $|G|$ denotes the cardinality of the set G. We define

DEFINITION 2.1.

$$\begin{array}{rcl} x \in \mathcal{F} & :\Longleftrightarrow & |\mathcal{N}_x| = 2 \\ x \in \mathcal{E} & :\Longleftrightarrow & |\mathcal{N}_x| \geq 3 \quad \textit{and} \quad \exists y \in \Gamma_h, y \neq x, \ \textit{such that } y \sim x \\ x \in \mathcal{V} & :\Longleftrightarrow & |\mathcal{N}_x| \geq 3 \quad \textit{and} \quad \nexists y \in \Gamma_h, \ \textit{such that } x \sim y. \end{array}$$

In the case of a decomposition into regular substructures, e.g., cubes or tetrahedra, our definition of faces, edges, and vertices is conform with our basic geometric intuition; see also Figure 6.1.

In the definition of dual-primal FETI methods, we need the notion of edge averages, and in the case of heterogeneous materials, also of edge first order moments. We note that the rigid body modes $\mathbf{r}_1, \ldots, \mathbf{r}_6$, restricted to a straight edge provide only five linearly independent vectors, since one rotation is always linearly dependent on other rigid body modes. For the following definition, we assume that we have used an appropriate change of coordinates such that the edge under consideration coincides with the x_1-axis and the special rotation is then $\mathbf{r}_6$. The edge averages and first order moments over this specific edge $\mathcal{E}$ are of the form

$$\frac{\int_{\mathcal{E}} \mathbf{r}_k^T \mathbf{u} dx}{\int_{\mathcal{E}} \mathbf{r}^T \mathbf{r} dx}, \quad k \in \{1, \ldots, 5\}, \mathbf{u} = (u_1^T, u_2^T, u_3^T)^T \in \mathbf{W}^h. \tag{2.4}$$

We note that on edges which are not straight, we can use all six rigid body modes to construct six average and first order moment constraints.

3. The FETI-DP algorithm. For each subdomain $\Omega_i, i = 1, \ldots, N$, we assemble local stiffness matrices $K^{(i)}$ and local load vectors $\mathbf{f}^{(i)}$. By $\mathbf{u}^{(i)}$ we denote the local solution vectors of nodal values.

In the dual-primal FETI methods, we distinguish between dual and primal displacement variables by the way the continuity of the solution in those variables is established. Dual displacement variables are those, for which the continuity is enforced by a continuity constraint and Lagrange multipliers $\boldsymbol{\lambda}$ and thus, continuity is not established until convergence of the iterative method is reached, as in the classical one-level FETI methods; see, e.g., [12]. On the other hand, continuity of the primal displacement variables is enforced explicitly in each iteration step by subassembly of the local stiffness matrices $K^{(i)}$ at the primal displacement variables. This subassembly yields a symmetric, positive definite stiffness matrix $\widetilde{K}$ which is coupled at the primal displacement variables but block diagonal otherwise. Let us note that this coupling yields a global problem which is necessary to obtain a numerically scalable algorithm.

We will use subscripts I, Δ, and Π, to denote the interior, dual, and primal displacement variables, respectively, and obtain for the local stiffness matrices, load

vectors, and solution vectors of nodal values

$$K^{(i)} = \begin{bmatrix} K_{II}^{(i)} & K_{\Delta I}^{(i)T} & K_{\Pi I}^{(i)T} \\ K_{\Delta I}^{(i)} & K_{\Delta\Delta}^{(i)} & K_{\Pi\Delta}^{(i)T} \\ K_{\Pi I}^{(i)} & K_{\Pi\Delta}^{(i)} & K_{\Pi\Pi}^{(i)} \end{bmatrix}, \mathbf{u}^{(i)} = \begin{bmatrix} \mathbf{u}_I^{(i)} \\ \mathbf{u}_\Delta^{(i)} \\ \mathbf{u}_\Pi^{(i)} \end{bmatrix}, \mathbf{f}^{(i)} = \begin{bmatrix} \mathbf{f}_I^{(i)} \\ \mathbf{f}_\Delta^{(i)} \\ \mathbf{f}_\Pi^{(i)} \end{bmatrix}.$$

We also introduce the notation

$$\mathbf{u}_B = [\mathbf{u}_I^T\ \mathbf{u}_\Delta^T]^T, \mathbf{f}_B = [\mathbf{f}_I^T\ \mathbf{f}_\Delta^T]^T, \mathbf{u}_B^{(i)} = [\mathbf{u}_I^{(i)\,T}\ \mathbf{u}_\Delta^{(i)\,T}]^T, \text{ and } \mathbf{f}_B^{(i)} = [\mathbf{f}_I^{(i)\,T}\ \mathbf{f}_\Delta^{(i)\,T}]^T.$$

Accordingly, we define

$$K_{BB} = \mathrm{diag}_{i=1}^N(K_{BB}^{(i)}),\ \ K_{BB}^{(i)} = \begin{bmatrix} K_{II}^{(i)} & K_{\Delta I}^{(i)T} \\ K_{\Delta I}^{(i)} & K_{\Delta\Delta}^{(i)} \end{bmatrix},\ \ K_{\Pi B} = [K_{\Pi B}^{(1)}, \ldots, K_{\Pi B}^{(N)}].$$

We note that K_{BB} is a block diagonal matrix. By subassembly in the primal displacement variables, we obtain

$$\widetilde{K} = \begin{bmatrix} K_{BB} & \widetilde{K}_{\Pi B}^T \\ \widetilde{K}_{\Pi B} & \widetilde{K}_{\Pi\Pi} \end{bmatrix},$$

where a tilde indicates the subassembled matrices and where

$$\widetilde{K}_{\Pi B} = [\widetilde{K}_{\Pi B}^{(1)}, \ldots, \widetilde{K}_{\Pi B}^{(N)}].$$

Introducing local assembly operators $R_\Pi^{(i)}$ which map from the local primal displacement variables $\mathbf{u}_\Pi^{(i)}$ to the global, assembled $\widetilde{\mathbf{u}}_\Pi$, we have

$$\widetilde{K}_{\Pi B}^{(i)} = R_\Pi^{(i)} K_{\Pi B}^{(i)}, \qquad \widetilde{\mathbf{u}}_\Pi = \sum_{i=1}^N R_\Pi^{(i)} \mathbf{u}_\Pi^{(i)}, \qquad \widetilde{K}_{\Pi\Pi} = \sum_{i=1}^N R_\Pi^{(i)} K_{\Pi\Pi}^{(i)} R_\Pi^{(i)T},$$

for $i = 1, \ldots, N$. Due to the subassembly of the primal displacement variables, Lagrange multipliers have to be used to enforce continuity only for the dual displacement variables $\mathbf{u}_\Delta$. We introduce a discrete jump operator $B = [O\, B_\Delta]$ such that the solution $\mathbf{u}_\Delta$, associated with more than one subdomain, coincides when $B\mathbf{u}_B = B_\Delta \mathbf{u}_\Delta = 0$ with $\mathbf{u}_B = [\mathbf{u}_I^T, \mathbf{u}_\Delta^T]^T$. Since we assume pointwise matching grids across the interface Γ, the entries of the matrix B can be chosen as $0, 1$, and -1. However, we will otherwise use all possible constraints and thus work with a fully redundant set of Lagrange multipliers as in [12, Section 5]; cf. also [17]. Thus, for an edge node common to four subdomains, we will use six constraints rather than choosing as few as three.

We can now reformulate the finite element discretization of (2.3) as

$$\begin{bmatrix} K_{BB} & \widetilde{K}_{\Pi B}^T & B^T \\ \widetilde{K}_{\Pi B} & \widetilde{K}_{\Pi\Pi} & O \\ B & O & O \end{bmatrix} \begin{bmatrix} \mathbf{u}_B \\ \widetilde{\mathbf{u}}_\Pi \\ \boldsymbol{\lambda} \end{bmatrix} = \begin{bmatrix} \mathbf{f}_B \\ \widetilde{\mathbf{f}}_\Pi \\ \mathbf{0} \end{bmatrix}. \tag{3.1}$$

Elimination of the primal variables $\widetilde{\mathbf{u}}_\Pi$ and of the interior and dual displacement variables $\mathbf{u}_B$ leads to a a reduced linear system of the form

$$F\boldsymbol{\lambda} = \mathbf{d},$$

where the matrix F and the right hand side $\mathbf{d}$ are formally obtained by block Gauss elimination, i.e., we have

$$\begin{aligned}\widetilde{S}_{\Pi\Pi} &= \widetilde{K}_{\Pi\Pi} - \widetilde{K}_{\Pi B} K_{BB}^{-1} \widetilde{K}_{\Pi B}^T, \\ F &= B K_{BB}^{-1} B^T + B K_{BB}^{-1} \widetilde{K}_{\Pi B}^T \widetilde{S}_{\Pi\Pi}^{-1} \widetilde{K}_{\Pi B} K_{BB}^{-1} B^T, \\ \mathbf{d} &= B K_{BB}^{-1} \mathbf{f}_B + B K_{BB}^{-1} \widetilde{K}_{\Pi B}^T \widetilde{S}_{\Pi\Pi}^{-1} \left(\widetilde{\mathbf{f}}_\Pi - \widetilde{K}_{\Pi B} K_{BB}^{-1} \mathbf{f}_B \right).\end{aligned}$$

Let us note that the matrix F is never built explicitly but that in every iteration appropriate linear systems are solved, that the first term of the sum on the right hand side of the representation of F applied to a vector can be computed completely in parallel since K_{BB} is a block-diagonal matrix, and that the second term in that sum contains our global problem needed for scalability; see [11] or [9] for further details.

To define the FETI-DP Dirichlet preconditioner M^{-1}, we introduce a scaled jump operator B_D; this is done by scaling the contributions of B associated with the dual displacement variables from individual subdomains. We define

$$B_D = [B_D^{(1)}, \ldots, B_D^{(N)}],$$

where the $B_D^{(i)}$ are defined as follows: each row of $B^{(i)}$ with a nonzero entry corresponds to a Lagrange multiplier connecting the subdomain Ω_i with a neighboring subdomain Ω_j at a point $x \in \partial\Omega_{i,h} \cap \partial\Omega_{j,h}$. We obtain $B_D^{(i)}$ by multiplying each such element of $B^{(i)}$ with

$$\delta_j^\dagger(x) := \frac{G_j(x)}{\sum_{k \in \mathcal{N}_x} G_k(x)}, \tag{3.2}$$

where $\mathcal{N}_x$ is the set of indices of subdomains which have x on its boundary. Our preconditioner is then given in matrix form by

$$M^{-1} = B_D R_\Gamma^T S R_\Gamma B_D^T = \sum_{i=1}^N B_D^{(i)} R_\Gamma^{(i)T} S^{(i)} R_\Gamma^{(i)} B_D^{(i)T}. \tag{3.3}$$

Here, $R_\Gamma^{(i)}$ are restriction matrices that restrict the degrees of freedom of a subdomain to its interface and $R_\Gamma = \mathrm{diag}_i(R_\Gamma^{(i)})$.

We have to decide how to choose the primal displacement variables. The simplest choice is to select them as certain primal vertices of the subdomains; see [7], where this approach was first considered; this version has been denoted by Algorithm A; see [13]. Unfortunately, this choice does not always lead to good convergence results in three dimensions. To obtain better convergence for three dimensional problems, a different coarse problem was suggested by introducing additional constraints. These constraints are averages or first order moments over selected edges or faces, cf. (2.4) for edges, which are enforced to have the same values across the interface. For further details, see [8], [11], or [9]. To obtain robust condition number bounds for highly heterogeneous materials, additional first order moments over selected edges have to be used; cf. [11].

An edge where at least one edge average of one displacement component is imposed as a primal constraint will be denoted as a *primal edge*. At most three average constraints can be imposed on such an edge. Furthermore, an edge, where three edge

averages over all three displacement components and additionally two or three edge first order moments are imposed as primal constraints will be denoted as a *fully primal edge*.

There are different ways of implementing these additional primal constraints. One is to use additional, optional Lagrange multipliers, see [8] or [11], another one is to apply a transformation of basis, see [11] and [9]. In our work, we use a transformation of basis. Let us note that this approach leads again to a mixed linear system of the form (3.1) and that the same algorithmic form as for Algorithm A can be used; see [11], [9], and [10] for further details.

From the inner products of $\mathbf{u}_E$ with the translational and the rotational rigid body modes, we obtain three averages and two or three first order moments, respectively; cf. (2.4). These averages and moments are explicitly introduced as new variables into the new basis and will form a part of the set of primal displacement variables. The dual displacement vectors in the new basis will have a zero edge average and will be orthogonal to the rotations on the fully primal edge under consideration; this can also be seen as having certain first order moments to be zero.

We now describe how the transformation matrix for such a change of basis can be constructed. Here, we restrict ourselves to the construction of the basis transformation for a single, fully primal edge; see [11] or [9] for a detailed, algorithmic description. We consider the six rigid body modes $\mathbf{r}_i, i = 1, \ldots, 6$; cf. Section 2. Next, we orthogonalize the rigid body modes on the edge against each other using a stable formulation of the Gram-Schmidt process, e.g., modified Gram-Schmidt. We note that the translational rigid body modes are already orthogonal to each other and thus, we only have to start with the rotations in order to obtain an orthogonal basis of rigid body modes on the edge $\mathcal{E}$. We denote the orthogonal basis obtained by this process by $(\hat{\mathbf{r}}_j)_{j=1,\ldots,\ell}$, with $\ell \in \{5, 6\}$. When restricted to a straight edge $\mathcal{E}$, one of the rotations is linearly dependent on the others and should vanish when modified Gram-Schmidt is used; cf. also the discussion at the end of Section 2. Then, we only have a five dimensional basis.

Let us assume that the vector of nodal unknowns $\mathbf{u}_E$ has length n. We then consider the set of vectors $\{(\hat{\mathbf{r}}_j)_{j=1,\ldots,\ell}, (\mathbf{e}_i)_{i=1,\ldots,n}\}$, where $\mathbf{e}_i$ is the unit vector with one at the i-th component and zero otherwise, which is associated with the i-th d.o.f. on the fully primal edge. Starting with the orthogonalized rigid body modes $(\hat{\mathbf{r}}_j)_{j=1,\ldots,\ell}$, we orthogonalize the set of $n + \ell$ vectors, using modified Gram-Schmidt. We discard the ℓ linearly dependent vectors and use the remaining n orthogonal vectors to define the column vectors of our transformation matrix T_E.

The transformation matrix T_E performs the desired change of basis from the new basis to the original nodal basis. Denoting the edge unknowns in the new basis by $\widehat{\mathbf{u}}_E$, we have

$$\mathbf{u}_E = T_E \widehat{\mathbf{u}}_E.$$

A similar construction can be carried out for an edge where only averages are used as primal constraints. Only edge averages are then introduced as new variables and the remaining new variables will have zero edge average. We note that in this case, we can also explicitly set up a transformation matrix for the basis transformation; see, e.g., [9].

In the theory presented in Klawonn and Widlund [11], it is assumed that the subdomains are polytopes with good aspect ratios and that the edges are straight. Furthermore, large material discontinuities should be aligned with the interface. For

our FETI-DP algorithm, using a well selected set of primal constraints of edge averages or first order moments and in some very difficult cases also primal vertices, we have the estimate, cf. [11],

THEOREM 3.1. *The condition number satisfies*

$$\kappa(M^{-1}F) \leq C\,(1+\log(H/h))^2.$$

Here, $C > 0$ is independent of h, H, and the values of the coefficients G_i.

Let us give some assumptions from [11] which are sufficient to obtain a condition number estimate as in Theorem 3.1. In [11, Section 5], the definition of a *fully primal face* is introduced as a face which has six edge constraints, averages or first order moments, on edges which belong to the boundary of that face, such that the rigid body modes on that face are controlled. A sufficient condition for Theorem 3.1, cf. [11, Section 8.2], is to assume that every face is fully primal, every edge which belongs to more than three subdomains is fully primal, and every vertex is primal. In fact, not every such edge and every face has to be fully primal as long as for every pair of subdomains $\{\Omega_i, \Omega_j\}$ which has a (not fully primal) face or edge in common, there is a path connecting them, possibly through several other subdomains Ω_k, passing only through fully primal faces, such that the stiffnesses G_k associated with Ω_k, are never smaller than the minimum of the stiffnesses associated with Ω_i and Ω_j.

Also typically not all vertices, have to be primal. A similar path concept as for shared edges and faces can be used; see [11, Section 5]. Here, we can be a bit more lenient. It is sufficient for an arbitrary pair of subdomains $\{\Omega_i, \Omega_j\}$ which have a (non primal) vertex in common, to have a connecting path of the same nature as before. The only difference is that we replace G_k by $\frac{H}{h}\,G_k$ in the definition of the path above.

A slightly more general result can be shown if a tolerance is introduced in the concept of acceptable paths; cf. [11] for more details.

4. Necessary and sufficient constraints. In order to control the rigid body motions of a subregion, we need at least six constraints. In [11, Section 5], two model problems are considered to develop an understanding of the type and number of necessary and sufficient constraints needed in order to obtain a robust and scalable domain decomposition method. Here, we present numerical results which support the theoretical findings in [11].

In both model problems, we consider the unit cube in $\mathbb{R}^3$, decomposed into a set of smaller, cubic subdomains with sidelength H. The unit cube is only fixed at one face and a volume force is applied. In all of our experiments, we use four node, tetrahedral finite elements. The Poisson ratio in our linear elasticity problem is always $\nu = 0.29$ and the Young modulus will be given separately for the different problems.

All computations were carried out using PETSc, see [3, 1, 2], on a 16 processor (2.2 Ghz dual Opteron 248; Gigabit Ethernet; 4 GB memory for each processor) computing cluster in Essen. On this hardware we use UMFPACK 4.3 [5] as local subdomain and coarse problem direct solver.

We first consider a decomposition of the unit cube into $3 \times 3 \times 4$ subdomains of 1 536 d.o.f. each, where we have two interior cubic subdomains made of the same material having a face in common and being surrounded by cubic subdomains made of a material with much smaller Young modulus; cf. Figure 4.1.

Here, we check if six constraints for a face are necessary. We start with making all edges of the decomposition primal, using all three edge averages, one for each displacement component, on each edge. Then, we successively reduce the number of constraints at that common face until no constraints are imposed anymore. Since we

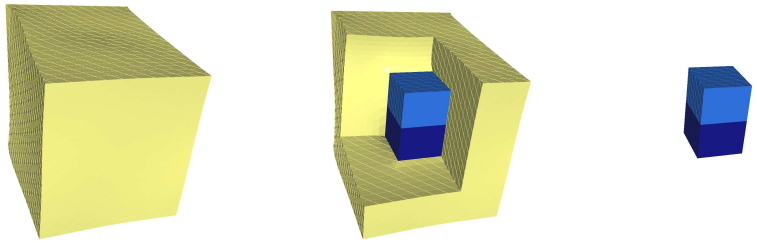

Fig. 4.1
Two stiff cubic subdomains sharing a face surrounded by softer material. Left: Unit cube; Middle: Unit cube cut open with two stiff subdomains inside; Right: Two stiff subdomains shown without surrounding softer material.

Fig. 4.2: Edges in a U-shaped, L-shaped, and parallel distribution.

always impose three average constraints on a primal edge, we first choose $12 = 4 \times 3$ averages, followed by $9 = 3 \times 3$, $6 = 2 \times 3$, $3 = 1 \times 3$, and 0 averages. From the numerical results presented in Table 4.1, we see that, for this constellation, six linearly independent constraints are necessary to obtain a robust domain decomposition method. We note that in the two cases of two primal edges considered here, we always have one linearly dependent constraint.

	# primal edges					
E_1/E_2	4	3 (U)	2 (L)	2 (II)	1	0
1	**9.75**	**10.11**	12.77	10.86	13.37	15.67
10^3	**9.24**	**24.28**	1.74×10^3	1.11×10^3	2.16×10^3	4.31×10^3
10^6	**9.24**	**24.64**	1.73×10^6	1.11×10^6	2.14×10^6	4.25×10^6

Table 4.1
Two stiff subdomains sharing a face $\mathcal{F}$. Condition number estimates for different numbers of edge average constraints. The notation U, L, and II denote a U-shaped, an L-shaped, and a parallel distribution of the primal edges of the face $\mathcal{F}$, cf. Figure 4.2. Young modulus: $E_2 = 210$; Stopping criterion: relative residual reduction by 10^{-10}. Primal constraints: Edge averages.

In the general theory developed in [11], we do not have to make every face fully primal but it is sufficient to have an acceptable path. Since we are not considering any experiments where the concept of an acceptable path is involved, we only refer to [11] for further details.

We next consider a model problem, where two subdomains are again surrounded by subdomains with much smaller stiffnesses, i.e., Young moduli. Furthermore, we

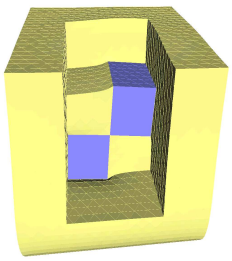

Fig. 4.3
Two stiff cubic subdomains sharing an edge surrounded by softer material. Unit cube Ω cut open in front and on top.

assume that these two special subdomains share only an edge; cf. Figure 4.3. In [11] it was shown that a well selected set of primal constraints, which has five linearly independent primal constraints related to that special edge shared by the two stiffer subdomains and otherwise six linearly independent edge constraints for each face, is sufficient to prove a condition number bound as in Theorem 3.1. In [11], the five linearly independent constraints are chosen as three edge averages and two properly chosen first order moments; cf. also (2.4). Here, the six linearly independent constraints for each face can be chosen as edge averages (and moments) over appropriately chosen edges of the considered face. In a set of experiments, we have tested different combinations of edge constraints on the specific edge shared by the two stiffer subdomains; cf. Table 4.2. In the case of three constraints only edge averages are used, in the case of five, additionally two first order moments are applied. On all other edges, an edge average over each displacement component is used to define the primal constraints. We see that using no constraints or only edge average constraints on the specific edge leads to a large condition number. Applying all five constraints leads to a good condition number which is bounded independently of the jump in the Young moduli.

From the theory in Klawonn and Widlund [11], it is expected that for the problem with just one bad edge, we only have two large eigenvalues which are outliers in an otherwise nicely clustered spectrum; this also explains the good iteration counts in Table 4.2. To confirm this numerically, we compute all eigenvalues for a small model problem. Here, the unit cube is decomposed into $2\times2\times2 = 8$ regular cubic subdomains with 1 029 d.o.f. each, resulting in 6 591 global d.o.f. We assume again that we have two stiff subdomains sharing an edge surrounded by softer material; cf. Figure 4.5. The ratio of the different Young moduli is $E_1/E_2 = 10^6$ with $E_2 = 210$. As constraints we impose three edge averages, one for each displacement component, on each edge but no primal vertices. In this case, we have a large condition number due to two outliers in the spectrum, related to the two rotations which are not controlled due to the missing first order moments; cf. Figure 4.4. If we remove those two outlying eigenvalues from the diagram, we see that the remaining spectrum is still nicely clustered, cf. the diagram on the right hand side in Figure 4.4. Next, we consider the case when two additional first order moments are imposed on the bad edge shared by the two stiffer subdomains. Here, the spectrum is nicely clustered and the ratio of the two extreme non-zero eigenvalues is bounded by a small number; cf. Figure 4.5.

Next, we analyze a more involved example with several bad edges, where we will

	−3			+0			+2		
E_1/E_2	It.	$\lambda_{\max}$	$\lambda_{\min}$	It.	$\lambda_{\max}$	$\lambda_{\min}$	It.	$\lambda_{\max}$	$\lambda_{\min}$
10^0	29	9.31	1.0111	28	9.20	1.0115	28	**9.19**	1.0113
10^1	31	12.13	1.0105	30	9.14	1.0099	30	**9.14**	1.0098
10^2	36	51.15	1.0115	31	10.61	1.0096	30	**9.11**	1.0094
10^3	47	4.41×10^2	1.0113	37	75.72	1.0081	30	**9.11**	1.0084
10^4	48	4.34×10^3	1.0191	41	7.27×10^2	1.0080	30	**9.10**	1.0080
10^5	65	4.33×10^4	1.0156	48	7.24×10^3	1.0080	30	**9.10**	1.0080
10^6	70	4.33×10^5	1.0215	47	7.24×10^4	1.0116	30	**9.10**	1.0080

Table 4.2

Straight edge: Unit cube decomposed into $3 \times 4 \times 4 = 48$ brick-shaped subdomains of 1 536 d.o.f. each, 55 506 total d.o.f., 75 edges, edges use three edge averages; one special edge: −3: no constraints on this edge, 0: only averages, +2: averages and, additionally, two first order moments; Stopping criterion: Relative residual reduction by 10^{-10}.

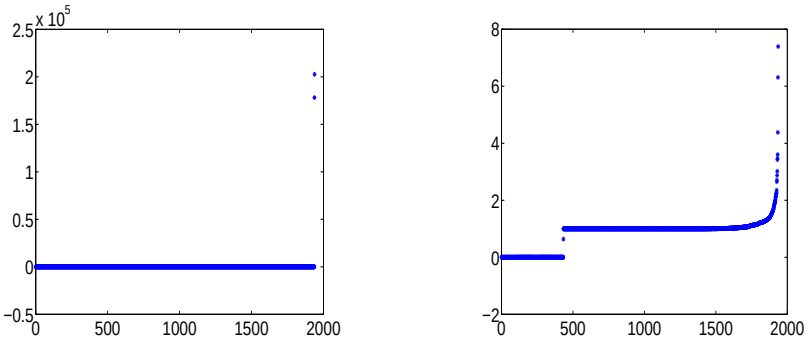

Fig. 4.4

Eigenvalues for FETI-DP using only edge averages, no primal vertices. Left: All eigenvalues. Right: All but the two largest eigenvalues.

see that additional first order moments not only improve the condition number but can be absolutely necessary to obtain convergence. We consider a linear elasticity model problem with a material consisting of different layers as shown in Figure 4.6, where the homogeneous layer is made of the softer material. The ratio of the different Young moduli is $E_1/E_2 = 10^6$ with $E_2 = 210$. Here, in addition to three edge averages on each edge, we have also used two first order moments as primal constraints on all edges. The results in Table 4 clearly show that the additional first order moments help to improve the convergence significantly; see [11] for theoretical results. In Table 4.4 the parallel scalability is shown for a cube of eight layers with a material distribution as in Figure 4.6.

Finally, we numerically check if primal vertex constraints are necessary at all. So far, all of our experiments were carried out without any primal vertices. In the theoretical analysis given in [11], it is shown that in some special situations, primal

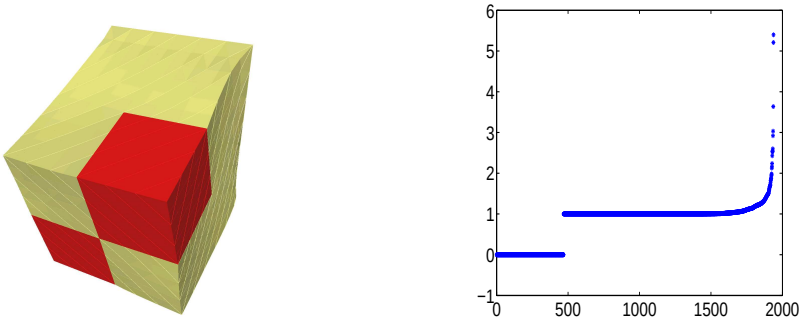

Fig. 4.5
Left: Two stiff cubic subdomains sharing a straight edge surrounded by softer material. Right: All eigenvalues for FETI-DP using edge averages and two first order moments on the shared edge, no primal vertices.

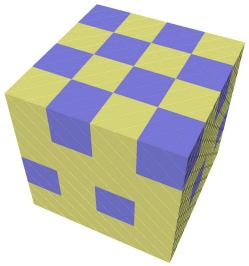

Fig. 4.6
Alternating layers of a heterogeneous material distributed in a checkerboard pattern and a homogeneous, softer material.

edge averages			edge averages + first order moments		
Cond.	It.	Time	Cond.	It.	Time
2.14×10^5	$>$ **1 000**	$>$ 6 686s	5.19	**24**	629s

Table 4.3
Heterogeneous linear elasticity: Comparison of FETI-DP algorithm using edge averages vs. edge averages and first order moments; Decomposition into $12 \times 12 \times 12 = 1\,728$ cubic subdomains of 5 184 d.o.f. each, resulting in 7 057 911 total d.o.f. Stopping criterion: Relative residual reduction of 10^{-10}.

vertices have to be introduced. We now construct such a model problem, following the theoretical considerations given in [11, Section 8.3]. We decompose the unit cube into $27 = 3 \times 3 \times 3$ cubic subdomains. The subdomains are made of two different materials, distributed such that subdomains of the same material type are only connected at the subdomain vertices; cf. Figure 4.7. From the results presented in Table 4.5, we conclude that there exist very hard cases of material distributions where we have to

Proc.	Subdomains/Proc.	It.	Cond.	Time
1	512	17	5.18	**1 828s**
2	256	17	5.18	**842s**
4	128	17	5.18	**428s**
8	64	17	5.18	**215s**
16	32	17	5.18	**122s**

Table 4.4
FETI-DP: Parallel scalability using edge averages and first order moments. 512 subdomains with 5 184 d.o.f. each, yielding 2 114 907 global d.o.f. Stopping criterion: Relative residual reduction of 10^{-7}.

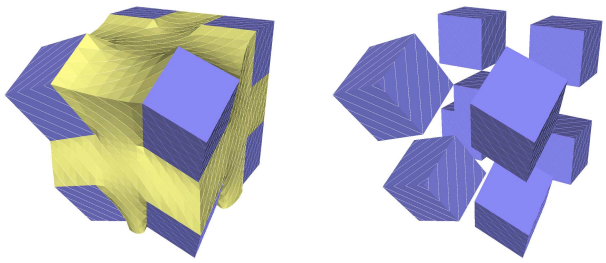

Fig. 4.7
Unit cube decomposed into 9 stiff subdomains, sharing only vertices, and 18 soft subdomains. Left: Deformation showing stiff and soft subdomains. Right: Deformation, showing only stiff subdomains.

introduce primal vertices. This confirms the theoretical findings given in Klawonn and Widlund [11]. The problem considered in the present example is of course somewhat artificial. If primal vertices have to be introduced in real, industrial engineering applications in order to obtain a robust algorithm, still has to be numerically tested with such problems.

5. Curved edges. In this section, we present numerical results for decompositions with curved edges. The theory in [11] is only for straight edges. We will see from the following numerical results that first order moments are still necessary in the case of large coefficient jumps.

In order to study the effect of slightly bent edges we start from the same configuration as in Table 4.2, i.e., with two stiff subdomains sharing an edge, surrounded by softer material with a Young modulus $E_2 = 210$. We note that in all of our experiments, the Poisson ratio is $\nu = 0.29$. We then consider a slightly bent cross section, cf. Figure 5.1, according to an inner radius of curvature of $1/\sqrt{2}, 1, \sqrt{2}$. We thus have a bent critical edge shared by the two stiff subdomains.

We start with a slightly bent configuration, corresponding to a radius of curvature of $1/\sqrt{2}$, as depicted in the leftmost picture of Figure 5.2. In Table 5.1 the effect is shown as we increase E_1 and the two subdomains become increasingly stiffer. We see

	edge averages + primal vertices		only edge averages	
E_1/E_2	It.	Cond.	It.	Cond.
1	26	**7.22**	26	7.56
10^3	23	**8.03**	49	89.58
10^6	24	**7.98**	113	8.38×10^4

Table 4.5
Comparison of FETI-DP using edge averages and vertices as primal constraints vs. a variant using only edge averages as primal constraints. Decomposition into $27 = 3 \times 3 \times 3$ subdomains, cf. Fig. 4.7, with 1 536 d.o.f. each, resulting in 31 944 global d.o.f. Stopping criterion: Relative residual reduction by 10^{-10}.

that starting from a certain point we cannot control the condition number anymore by using only two first order moments on the edge. Nevertheless, if we choose the right two moments, denoted as "good choice" in Table 5.1, the condition number is controlled much longer than in the case where we make the wrong choice, captioned "bad choice". If we introduce all three moments as constraints for a bent edge then the condition number stays small independently of the ratio E_1/E_2.

We then study the effect of different curvatures on the condition number and on the necessity to add all three moments to the constraints. In Table 5.2 we only consider three values for E_1/E_2, namely unity, 10^3 and 10^6. We include the case $E_1/E_2 = 1$, i.e., the case of homogeneous material, to verify that the deformation of the unit cube only has a minor effect on the condition number and iteration count. This is the case whether we use two moments or three as long as we have a homogeneous material.

We also find that for $E_1/E_2 = 10^3$ we do not see any difference between using two and three constraints even if we bent the edge to a radius of curvature of $1/\sqrt{2}$ as depicted in the rightmost picture of Figure 5.2.

Only for $E_1/E_2 = 10^6$, we see that two constraints are not sufficient anymore and we have to introduce the third linearly independent moment as additional constraint in order to control the condition number and iteration count.

The fact that the iteration count is smaller in the case where only two moments are introduced as constraints and $E_1/E_2 = 10^6$, cf. Table 5.2, is an artifact of our stopping criterion. This is also the reason for some of the low iteration counts in Table 5.1 in the cases where we have very high condition numbers. We have a residual reduction of 10^{-10} but the starting residual is exceptionally high in these cases. Note that this effect only occurs when the condition number of the problem becomes very large.

From these numerical results, we conclude that discontinuities in the material stiffnesses of the order of 10^3 can still be treated using three edge averages and two first order moments. To obtain an unconditionally robust method, our experiments seem to indicate that, in the case of edges which are not straight, three edge averages and three first order moments are needed.

6. Material heterogeneities not aligned with the interface. In the theoretical estimates presented in [11], it is assumed, as it is standard in theoretical analyses of this type, that the coefficient jumps of the Young moduli are aligned with the interface, i.e., discontinuities can only occur across the subdomain boundaries. In practice, satisfying such an assumption can lead to a decomposition with very bad

	+2 (bad choice)			+2 (good choice)			+3		
E_1/E_2	It.	$\lambda_{\max}$	$\lambda_{\min}$	It.	$\lambda_{\max}$	$\lambda_{\min}$	It.	$\lambda_{\max}$	$\lambda_{\min}$
10^0	35	13.03	1.0103	35	13.03	1.0103	35	**13.03**	1.0103
10^1	34	12.70	1.0098	34	12.70	1.0098	34	**12.70**	1.0098
10^2	35	12.60	1.0091	34	12.57	1.0093	34	**12.57**	1.0094
10^3	38	61.55	1.0083	35	12.53	1.0077	35	**12.53**	1.0078
10^4	43	5.71×10^2	1.0072	34	12.54	1.0082	34	**12.52**	1.0082
10^5	49	5.67×10^3	1.0064	35	43.67	1.0104	37	**12.51**	1.0069
10^6	54	5.67×10^4	1.0060	33	4.02×10^2	1.0156	39	**12.51**	1.0061

Table 5.1
Curved edge: Deformed unit cube decomposed into $3 \times 4 \times 4 = 48$ brick-shaped subdomains of 1 536 d.o.f. each, radius of curvature $1/\sqrt{2}$, special edge is curved, 55 506 total d.o.f., relative tolerance 10^{-10}; 75 edges, edges use three edge averages; one special edge: +2: averages and, additionally, two first order moments, +3: averages and, additionally, three first order moments; Young modulus $E_2 = 210$.

	Radius of	+2			+3		
E_1/E_2	curvature	It.	$\lambda_{\max}$	$\lambda_{\min}$	It.	$\lambda_{\max}$	$\lambda_{\min}$
	straight	28	9.19	1.0113			
	$\sqrt{2}$	31	9.99	1.0106	31	**9.99**	1.0106
10^0	1	32	10.66	1.0105	32	**10.66**	1.0105
	$1/\sqrt{2}$	35	13.03	1.0103	35	**13.03**	1.0103
	straight	30	9.11	1.0084			
	$\sqrt{2}$	32	9.80	1.0075	31	**9.80**	1.0082
10^3	1	33	10.45	1.0074	32	**10.45**	1.0080
	$1/\sqrt{2}$	35	12.53	1.0077	35	**12.53**	1.0078
	straight	30	9.10	1.0080			
	$\sqrt{2}$	28	1.01×10^2	1.0153	35	**9.79**	1.0065
10^6	1	30	2.00×10^2	1.0150	35	**10.45**	1.0063
	$1/\sqrt{2}$	33	4.02×10^2	1.0156	39	**12.51**	1.0061

Table 5.2
Curved edge: Deformed unit cube decomposed into $3 \times 4 \times 4 = 48$ brick-shaped subdomains of 1 536 d.o.f. each, radius of curvature $1/\sqrt{2}$, special edge is curved, 55 506 total d.o.f., relative tolerance 10^{-10}; 75 edges, edges use three edge averages; one special edge: +2: averages and, additionally, two first order moments, +3: averages and, additionally, three first order moments; Young modulus $E_2 = 210$.

aspect ratios which usually spoil the convergence rate. In this section, we numerically analyze the effect of material heterogeneities which are not aligned with the interface. We first apply our algorithm with edge averages, but without first order

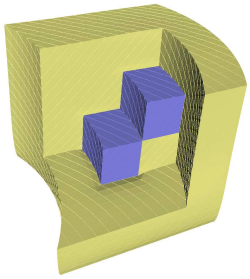

Fig. 5.1
Deformed unit cube (radius of curvature = 1) with two deformed stiff subdomains sharing a curved edge surrounded by softer material.

Fig. 5.2
Curved configurations seen from bottom, radius of curvature = $\sqrt{2}$, 1, $1/\sqrt{2}$.

moments and primal vertices, to four different model problems. We always consider a unit cube which is fixed at one face. In our experiments we always compare the case of a homogeneous material to different distributions of materials with different stiffness. We assume that the softer material has a Young modulus of $E_2 = 210$ and a Poisson ratio of $\nu = 0.29$. The Young modulus of the stiffer material is denoted by E_1 and the ratio of both is $E_1/E_2 = 10^6$. We use four node tetrahedral elements, a decomposition into $2 \times 2 \times 2 = 8$ cubic subdomains with 89 373 d.o.f. each, resulting in 680 943 global d.o.f. As stopping criterion, we use the relative residual reduction by 10^{-10}. In the first three experiments, the parts of Ω which consist of the stiffer material, do not intersect any interior edges; cf. Figures 6.1, 6.2, 6.3, 6.4. We note that these examples are constructed such that the material cannot be treated by the standard scaling, see (3.2), since the material discontinuity is not across the interface. From the results given in Tables 6.1, 6.2, and 6.3, we see that such a jump in the Young modulus seems not to affect severely the condition and iteration number.

Next, we consider an example, where a stiff cube is located at the center of a larger cube made out of a softer material; cf. Figure 6.5. The essential difference in comparison to the previous examples is that the stiffer subcube now intersects the interior edges; see also Figure 6.1. From the results given in the mid-column of Table 6.4, we see that this severely affects the iteration and condition number. As a remedy,

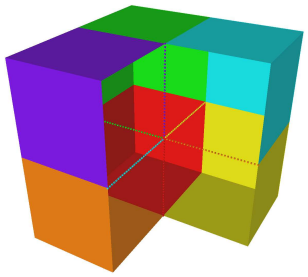

Fig. 6.1
For $2 \times 2 \times 2 = 8$ subdomains, the 6 edges in the interior of Ω are shown (two subdomains in front of the cube are not displayed).

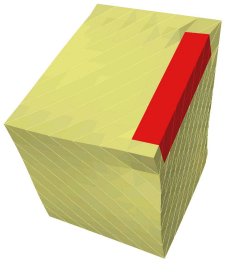

Fig. 6.2
Material heterogeneities not aligned with the interface. Soft cube (Young modulus $E_2 = 210$) with a stiff beam (Young modulus $E_1 = 10^6 \cdot E_2$), with square cross section, at the upper right edge.

Homogeneous		Heterogeneous	
It.	Cond.	It.	Cond.
31	18.62	42	32.59

Table 6.1
Iteration counts and condition number estimates for problem given in Figure 6.2. Homogeneous: $E_1 = E_2 = 210$. Heterogeneous: $E_2 = 210, E_1 = 10^6 \cdot E_2$.

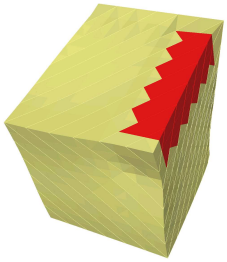

Fig. 6.3
Material heterogeneities not aligned with the interface. Soft cube (Young modulus $E_2 = 210$) with a stiff beam (Young modulus $E_1 = 10^6 \cdot E_2$), with square cross section and a jagged interface, at the upper right edge.

Homogeneous		Heterogeneous	
It.	Cond.	It.	Cond.
31	18.62	43	34.16

Table 6.2
Iteration counts and condition number estimates for problem given in Figure 6.3. Homogeneous: $E_1 = E_2 = 210$. Heterogeneous: $E_2 = 210, E_1 = 10^6 \cdot E_2$.

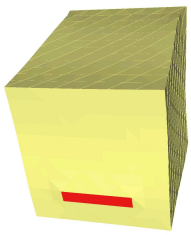

Fig. 6.4
Material heterogeneities not aligned with the interface. Soft cube (Young modulus $E_2 = 210$) with a stiff beam (Young modulus $E_1 = 10^6 \cdot E_2$), with rectangular cross section, at the upper right edge.

Homogeneous		Heterogeneous	
It.	Cond.	It.	Cond.
31	18.62	40	22.99

Table 6.3
Iteration counts and condition number estimates for problem given in Figure 6.4. Homogeneous: $E_1 = E_2 = 210$. Heterogeneous: $E_2 = 210, E_1 = 10^6 \cdot E_2$.

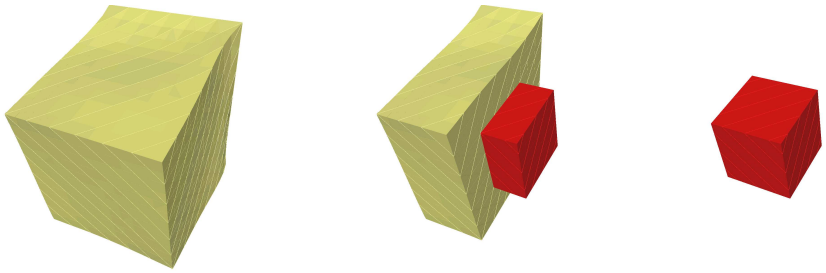

Fig. 6.5
Material heterogeneities not aligned with the interface. Soft material (Young modulus $E_2 = 210$) surrounding a stiffer cube (Young modulus $E_1 = 10^6 \cdot E_2$), centered at the origin of the cube. The stiffer, interior cube intersects with all interior edges.

we introduce a weighted edge average of the form

$$\frac{\sum_{x_i \in \mathcal{E}^h} \rho(x_i)\, u_j(x_i)}{\sum_{x_i \in \mathcal{E}^h} \rho(x_i)}, \quad j = 1, 2, 3, \tag{6.1}$$

with weights $\rho(x_i)$ defined pointwise by the maximum material stiffness at that point and $\mathbf{u} = [u_1^T, u_2^T, u_3^T]^T$. We note that this weighted edge average is reduced to the standard edge average in the case of material jumps aligned with the interface. The results given in the column on the right hand side of Table 6.4 indicate that this weighted edge average could be helpful in cases where the material discontinuities do not align with the interface. This should be further analyzed for more difficult problems coming from real-world, engineering examples.

7. Conclusions. We have presented a FETI-DP algorithm for elasticity problems with large jumps in the material stiffness. This method was introduced and theoretically analyzed in [11] and the results shown in Section 4 for straight edges

Edge average (hom.)		Edge average (het.)		Weighted average (het.)	
It.	Cond.	It.	Cond.	It.	Cond.
31	18.62	179	4.11×10^6	37	16.57

Table 6.4
Comparison of standard and weighted edge averages for the problem given in Figure 6.5. Decomposition into $8 = 2 \times 2 \times 2$ cubic subdomains with 89 373 d.o.f. each, yielding 680 943 global d.o.f. Stopping criterion: Relative residual reduction by 10^{-10}. Primal constraints: edge averages.

confirm the theoretical findings in [11]. We also considered curved edges in Section 5 and the results show that for moderate jumps in the Young modulus and slightly bent edges, it is sufficient to use two first order moments. For arbitrarily large jumps, we advocate the use of all three first order moments. Another important situation, which can usually not be covered by theoretical investigations, is the case when the material discontinuities are not aligned with the interface. Our numerical results indicate that such a material distribution seems not to affect the condition number and the iteration count, if the discontinuity does not appear on an interior edge. On the other hand, if the discontinuity appears on an interior edge, in the experiment considered in this paper, a weighted edge average was a remedy. Since this weighted average can be implemented without additional cost, we suggest it as the default setting. Further, extensive numerical tests for real-world, industrial engineering problems should be pursued.

REFERENCES

[1] Satish Balay, Kris Buschelman, Victor Eijkhout, William D. Gropp, Dinesh Kaushik, Matthew G. Knepley, Lois Curfman McInnes, Barry F. Smith, and Hong Zhang. PETSc users manual. Technical Report ANL-95/11-Revision 2.1.5, Argonne National Laboratory, 2004.

[2] Satish Balay, Victor Eijkhout, William D. Gropp, Lois Curfman McInnes, and Barry F. Smith. Efficient management of parallelism in object oriented numerical software libraries. In E. Arge, A. M. Bruaset, and H. P. Langtangen, editors, *Modern Software Tools in Scientific Computing*, pages 163–202. Birkhäuser Press, 1997.

[3] Satish Balay, William Gropp, Lois Curfman McInnes, and Barry Smith. PETSc World Wide Web home page. http://www.mcs.anl.gov/petsc/petsc.html, April 1996.

[4] Philippe G. Ciarlet. *Mathematical Elasticity Volume I: Three–Dimensional Elasticity.* North-Holland, 1988.

[5] Timothy A. Davis. A column pre-ordering strategy for the unsymmetric-pattern multifrontal method. *ACM Transactions on Mathematical Software*, 30(2):165–195, June 2004.

[6] Clark R. Dohrmann. A preconditioner for substructuring based on constrained energy minimization. *SIAM J. Sci.Comput.*, 25(1):246–258, 2003.

[7] Charbel Farhat, Michel Lesoinne, Patrick LeTallec, Kendall Pierson, and Daniel Rixen. FETI-DP: A dual-primal unified FETI method - part i: A faster alternative to the two-level FETI method. *Int. J. Numer. Meth. Engrg.*, 50:1523–1544, 2001.

[8] Charbel Farhat, Michel Lesoinne, and Kendall Pierson. A scalable dual-primal domain decomposition method. *Numer. Lin. Alg. Appl.*, 7:687–714, 2000.

[9] Axel Klawonn and Oliver Rheinbach. A parallel implementation of Dual-Primal FETI methods for three dimensional linear elasticity using a transformation of basis. Technical Report SM-E-601, Department of Mathematics, Universität Duisburg-Essen, Germany, February 2005. Schriftenreihe des Fachbereichs Mathematik; http://www.uni-essen.de/ingmath/Axel.Klawonn/TR-SM-E-601.pdf.

[10] Axel Klawonn and Oliver Rheinbach. Some computational results for robust FETI-DP methods applied to heterogeneous elasticity problems in 3D. In *Domain Decomposition Methods*

in Science and Engineering, Lecture Notes in Compuational Science and Engineering. Springer-Verlag, 2005. Accepted for publication in the proceedings of the 16th International Conference on Domain Decomposition Methods, New York City, January 11-14, 2005.

[11] Axel Klawonn and Olof Widlund. Dual-Primal FETI methods for linear elasticity. Technical report, Department of Computer Science, Courant Institute of Mathematical Sciences, New York University, New York, USA, September 2004. http://cs.nyu.edu/csweb/Research/TechReports/TR2004-855/TR2004-855.pdf.

[12] Axel Klawonn and Olof B. Widlund. FETI and Neumann–Neumann iterative substructuring methods: Connections and new results. *Comm. Pure Appl. Math.*, 54:57–90, January 2001.

[13] Axel Klawonn, Olof B. Widlund, and Maksymilian Dryja. Dual-Primal FETI methods for three-dimensional elliptic problems with heterogeneous coefficients. *SIAM J.Numer.Anal.*, 40, 159-179 2002.

[14] Jing Li and Olof B. Widlund. FETI-DP, BDDC, and Block Cholesky Methods. Technical Report TR2004-857, Department of Computer Science, Courant Institute of Mathematical Sciences, New York University, December 2004. http://cs.nyu.edu/csweb/ /Research/TechReports/TR2004-857/TR2004-857.pdf.

[15] Jan Mandel and Clark R. Dohrmann. Convergence of a balancing domain decomposition by constraints and energy minimization. *Numer. Lin. Alg. Appl.*, 10:639–659, 2003.

[16] Jan Mandel, Clark R. Dohrmann, and Radek Tezaur. An algebraic theory for primal and dual substructuring methods by constraints. *Appl. Numer. Math.*, 2004. Sixth IMACS International Symposium on Iterative Methods in Scientific Computing, Denver, Colorado, USA, 2003. To appear.

[17] Daniel Rixen and Charbel Farhat. A simple and efficient extension of a class of substructure based preconditioners to heterogeneous structural mechanics problems. *Int. J. Numer. Meth. Engrg.*, 44:489–516, 1999.

[18] Andrea Toselli and Olof B. Widlund. *Domain Decomposition Methods – Algorithms and Theory*, volume 34 of *Springer Series in Computational Mathematics*. Springer-Verlag, Berlin Heidelberg New York, 2005.